Article (refereed) - postprint

White, S.M.; Burden, J.P.; Maini, P.K.; Hails, R.S.. 2012 Modelling the within-host growth of viral infections in insects. *Journal of Theoretical Biology*, 312. 34-43. 10.1016/j.jtbi.2012.07.022

Modelling the within-host growth of viral infections in insects

S.M. White[a,b,1,*], J.P. Burden[a], P.K. Maini[b,c], R.S. Hails[a]

[a] *Centre for Ecology & Hydrology, Maclean Building, Benson Lane, Crowmarsh Gifford, Wallingford, Oxfordshire, OX10 8BB, United Kingdom.*
[b] *Centre for Mathematical Biology, Mathematical Institute, University of Oxford, 24-29 St Giles', Oxford, Oxfordshire, OX1 3LB, United Kingdom.*
[c] *Oxford Centre for Integrative Systems Biology, Department of Biochemistry, South Parks Road, Oxford, OX1 3QU, United Kingdom.*

Abstract

Insects are infected by a variety of pathogens, including bacteria, fungi and viruses, which have been studied largely for their potential as biocontrol agents, but are also important in insect conservation (biodiversity) and as model systems for other diseases. Whilst the dynamics of host-pathogen interactions are well-studied at the population level, less attention has been paid to the critical within-host infection stage. Here, the reproductive rate of the pathogen is largely determined by how it exploits the host; the resources supplied by the host in terms of size and condition; competition with other pathogens; and the speed with which it kills the host (death being an inevitable outcome for obligate-killing pathogens). In this paper we aim to build upon recent developments in the literature by conducting single infection bioassays to obtain data on growth and fitness parameters

*Corresponding author
Email addresses: smwhit@ceh.ac.uk (S.M. White), jbur@ceh.ac.uk (J.P. Burden), maini@maths.ox.ac.uk (P.K. Maini), rha@ceh.ac.uk (R.S. Hails)
[1] Tel: +44 (0)1491 692699; Fax: +44 (0)1491 692424

for phenotypically different and similar strains of nucleopolyhedroviruses in the Lepdipoteran host *Spodoptera exigua*. Using these data, a simple mechanistic mathematical model (a coupled system of differential equations) is derived, fitted and parameter sensitivity predictions are made which support empirical findings. We unexpectedly found that initial growth of virus within the host occurs at a double-exponential rate, which contrasts with empirical findings for vertebrate host-pathogen systems. Moreover, these infection rates differ between strains, which has significant implications for the evolution of virulence and strain coexistence in the field, which are still relative unknowns. Furthermore, our model predicts that, counter to intuition, increased viral doses may lead to a decrease in viral yield, which is supported by other studies. We explain the mechanism for this phenomenon and discuss its implications for insect host-pathogen ecology.
Keywords: Lepidoptera, nucleopolyhedrovirus, consumer-resource dynamics, biocontrol, baculovirus

1. Introduction

Pathogens play an important role for many host organisms, ranging from population regulation [1] to species invasion [2]. These in turn, have applications for our understanding of issues such as disease control [3], pest control [4] and biodiversity [5]. However, much of our empirical understanding of host-pathogen ecology and evolution is derived at the population level (see Dwyer et al. [6] for example), and the crucial pathogen stages operating within the host are either simply over-looked or assumed to be non-dynamic, whereas, in reality, key pathogen fitness and virulence traits are often de-

termined throughout the course of infection (e.g. environmental conditions). For example, in the case of monarch butterflies, *Danaus plexippus*, rearing infected larvae on different plant species alters parasite infection, replication and virulence [7]. This illustrates that population dynamics of hosts and pathogens will be subject to feedback mechanisms from the pathogen dynamics within the host.

This point is now being addressed by a number of authors, especially via theoretical means. For example, Antia and Lipsitch [8] proposed a mathematical model for an acute microparasite infection in a vertebrate host. This model suggested that the within-host dynamics of the microparasite will be a 'race' between parasite multiplication and the clonally expanding response by the host immune system, resulting either in immune-mediated clearance or host death. In a mathematically similar, but biologically different system, Ellner et al. [9] modelled the within-host interaction of a fungal pathogen in a coral. Here the fungal-immune system dynamics are rather complex and spatially explicit, highlighting the importance of 'immune response free space' which allows local rapid growth of the fungal infection. One application of these types of models has been to improve our understanding of pathogen evolution, which has revealed that the dynamics of the immune system may select for parasites with intermediate within-host growth rates, as this is when the number of transmission stages from infected hosts reaches a maximum [10].

A large proportion of previous theoretical models based the infection dynamics on Lotka-Volterra interactions (see Alizon and van Baalen [11] for an example and references therein) or models with a fixed kill rate by immunity

[12] and are aimed at vertebrate hosts, largely due to the applicability to human health. In contrast, little work has been carried out for invertebrate systems, particularly with empirical data to test the model.

The dynamics of pathogens within invertebrate hosts differ significantly from those of vertebrates. Firstly, many insect pathogens are obligate killers, in the sense that effective horizontal transmission may only be attained by the death of the host, whereas for most vertebrates the infectious stages are emitted throughout the course of infection. Secondly, since the host itself is simply a resource for the virus to reproduce, the size and growth rate of the host is crucial in determining the speed of pathogen replication and the yield of infectious stages. Lastly, common to both vertebrates and invertebrates, are innate immune mechanisms that can be either constitutively expressed or induced on exposure to infection [13]. However, invertebrates lack acquired immune responses, but their mechanistically simple innate effectors are functionally sophisticated and can be highly efficient [14]. Therefore, the vertebrate models do not lend themselves readily to invertebrate systems.

Ebert and Weisser [15] proposed a model for the dynamics of the within-host growth of obligate-killing parasites, such as baculoviruses, and many species of bacteria, bacteriophages, nematodes, fungi and microsporidia. Their model assumes that pathogen biomass grows logistically, where the carrying capacity (invertebrate host mass) is time-dependent (also assumed to be logistic in growth) and crucially does not depend on the extent of infection within the host. It is possible, however, that as the pathogen spreads through host tissues it would interfere with metabolic processes and ultimately inhibit the growth of the host. In this case, the host size at the time of death, and

therefore the 'pathogen carrying capacity' of the host, should depend on the extent of host tissue infection. Typically, this is not the case in vertebrate infections, and so the interaction between virus replication and host growth rates has not been explicitly considered. In this paper we aim to address this by developing a more biologically detailed model for the within-host growth of obligate killing viruses of invertebrates, which is parameterised and validated against experimental data.

We base our model on baculoviruses, a group of double stranded DNA obligate killing viruses, which have been particularly well studied because of their utility as expression vectors and biocontrol agents [16]. Baculoviruses can be subdivided into two distinct genera, Granuloviruses (GVs) and Nucleopolyhedroviruses (NPVs - the focus of this paper), and are indirectly transmitted pathogens, persisting outside their arthropod hosts as occlusion bodies (OBs), a proteinaceous matrix in which the virus particles are embedded. The OBs may contain many virus genomes. Hosts (primarily Lepidoptera) become infected by consuming OBs when eating foliage. The protein dissolves in the alkaline gut of the caterpillar allowing viruses to cross the gut wall and then to start replicating. Overt infections result in the death of the host a few days later. Body tissues are then dissolved with millions of virus particles being produced as a result. These OBs persist in the environment until consumed by a new host or are degraded by environmental factors.

In this paper, we begin by describing bioassays carried out with lepidopteran hosts, in which we determine key life-history traits of the baculovirus and the within-host growth rate of the different strains of virus. We

empirically explore the possibility that the virus infection may impede host growth rate, and whether this inhibition increases as the infection progresses using statistical models. We then develop a novel mathematical model for the within-host growth of the different strains of virus. This model incorporates the interactions observed and is parameterised by experimental data. The ecological implications are then discussed.

2. Infection Bioassays and Results

2.1. Materials & Methods

2.1.1. Insect and virus stocks

Spodoptera exigua larvae were reared in continuous culture on artificial diet [17]. Four different baculoviruses were used in this study; the Oxford strain of *Mamestra brassicae* nucleopolyhedrovirus (*Mb*NPV) [18], *Panolis flammea* nucleopolyhedrovirus (*Pafl*NPV) variant 4 [19], *Autographa californica* nucleopolyhedrovirus (*Ac*NPV) strain C6 [20] and *Spodoptera exigua* nucleopolyhedrovirus (*Se*NPV) [21]. Additional details can be found in the electronic supplementary material (ESM).

2.1.2. Determination of median lethal dose and mean time to death

Three blocked bioassays were carried out to determine the median lethal concentration (LC_{50}) and mean time to death of the four viruses in *S. exigua*. Newly moulted third instar larvae of *S. exigua* were selected on the basis of head capsule diameter and starved overnight at 28°C. Thirty insects per treatment were then dosed by droplet feeding [22] with 1μl of the virus concentrations specified. The time taken to administer each treatment was

recorded and the start time (T_0) taken as the mid-point of this. The exposed larvae were transferred to individual pots of artificial diet and reared at 28°C and checked after 24 hours, at which point any handling deaths were removed. The larvae were subsequently checked every 12 hours until death or pupation (if the host survived infection) and any levels of mortality and time to death recorded. Details of our statistical methods can be found in the ESM.

2.1.3. Measurement of the within host-growth of baculoviruses

Based on the data generated in the previous bioassays a virus concentration of 1×10^7 OBs/ml was selected for all four viruses as at this dose all insects should be infected. Newly moulted third instar *S. exigua* larvae were starved overnight and 200 larvae dosed with 1μl of either *Ac*NPV, *Mb*NPV, *Pafl*NPV or *Se*NPV virus at a concentration of 1×10^7 OBs/ml. The larvae were transferred to individual pots of artificial diet and reared at 28°C. After 2 hours ten larvae were collected from each treatment. These were then weighed and frozen at -20°C until DNA extraction. The process of weighing and freezing 10 individual larvae was repeated at 12 hour intervals until all remaining larvae had died from virus infection.

Details of the DNA extraction and quantification can be found in the ESM.

2.2. Bioassay Results

2.2.1. Infectivity and speed of kill of AcNPV, MbNPV, PaflNPV and SeNPV in third instar larvae of S. exigua

The mortality of third instar larvae of *S. exigua* was significantly different between the viruses ($\chi^2 = 98.1$, df = 4, p$\leq$0.001) although there was no significant difference between the mortality induced by *Ac*NPV and *Mb*NPV ($\chi^2 = 1.42$, df=1, p=0.233) (see Figure S1 (a) in the ESM). The mortality was significantly affected by dose of virus ($\chi^2 = 185.4$, df=1, p<0.001) but there was no significant interaction between dose and virus ($\chi^2 = 6.59$, df=4, p=0.159). Overall *Se*NPV showed the highest mortality and *Pafl*NPV showed the lowest mortality, and in all cases mortality increased with dose.

Time to death was significantly different between the viruses (see Figure S1 (b) in the ESM), with a significant interaction between virus dose and virus strain ($F_{4,799}$=16.59, p$\leq$0.001). The time to death of *Ac*NPV, *Mb*NPV and *Se*NPV decreased with increasing virus dose, however the slope of the line for *Pafl*NPV was not significantly different from zero ($F_{2,797}$=1.355, p=0.259) showing that the speed of kill of this virus was unaffected by dose.

2.2.2. Host growth and the within-host growth of baculoviruses in third instar larvae of S. exigua

Host weight showed distinct differences between infected and uninfected insects (see Figure 1). Growth rates are curvilinear with time (minimally adequate statistical models), and the degree of this curvilinearity varies with virus strain (virus*time^3, $F_{4,594}$=3.41, p=0.009) indicating that different strains impede host growth to varying degrees. The uninfected larvae grow to their peak in mass before a decrease in weight due to larvae preparing for

pupation (Figure 1 (e)). All infected larvae are smaller in mass in comparison with uninfected larvae, particularly at the later stages of infection prior to virus induced death. Both *Ac*NPV and *Mb*NPV infected larvae showed a similar decrease in host mass to controls at the latter stages of infection (Figure 1 (a)-(b)), but no such effect was shown for *Pafl*NPV and *Se*NPV (Figure 1 (c)-(d)).

Taking the first 7 census host growth data points from each treatment, when the $\log_{10}$ weight grows linearly with time (Figure 1 (f) - minimally adequate statistical model), the infected hosts (as one category) show a significantly slower initial growth rate than their uninfected counterparts ($F_{1,345} = 6.813$, p=0.009). Furthermore, the growth rates of control and infected larvae were individually compared (virus*time, $F_{4,339}$=4.617, p=0.001) indicating that NPV viral infections alter the growth of the host differentially during the early stages of infection. *Pafl*NPV and *Se*NPV infected larvae showed significantly reduced initial growth rates compared to the uninfected larvae (virus*time, $t_{1,339} = 3.645$, p=0.0003 and $t_{1,339} = 3.039$, p=0.003, respectively). Interestingly, *Ac*NPV and *Mb*NPV infected individuals showed no significant difference in initial growth rates when compared to their uninfected conspecifics.

The growth of the viruses within *S. exigua*, as measured by the proportion of total DNA represented by viral DNA, also varied significantly between the four viruses (see Figure 2). This relationship is highly non-linear and the degree of non-linearity varies (virus*time^5, $F_{3,594}$=3.19, p=0.025). All viral treatments showed a log sigmoidal relationship with time, with all treatments approaching an asymptotic proportion of DNA. Moreover, all treatments also

showed a decrease in the proportion of viral DNA shortly after inoculation, with *Se*NPV and *Ac*NPV showing the greatest reduction (approximately a 10-fold reduction). The four viruses also showed differences in the maximum proportion of the host they converted to virus biomass. *Ac*NPV had the highest ratio of virus to host DNA with a peak of 45%. *Se*NPV was unable to replicate as much viral DNA, peaking at 12.5%. *Mb*NPV and *Pafl*NPV had the slowest speeds of kill and lowest proportion of viral DNA (8% and 10% respectively).

3. Within-Host Virus Growth Mathematical Model

Using the statistical model fitting above we have been able to demonstrate differences in the growth dynamics of the 4 strains of virus within the host. However, this analysis does not inform us of the importance of various mechanisms and factors of viral infection. To address this we derive the mathematical model below.

3.1. The Model

Let $H(t)$ and $V(t)$ be the mass of healthy host tissue and mass of virus within the host at time t, respectively. We assume that the host is an invertebrate and thus has no acquired immunity [23]. Here, we only consider overt infections where the initial dose of virus is sufficiently large such that the innate immune response is negligible and cannot clear the infection, leading to host death. The host grows with growth rate $r(t)$. Note that since we are only interested in overt infections, it is not necessary to consider host growth in the absence of infection, where the dynamics are considerably different (e.g. overt infections will prevent the onset of pupation). Healthy host mass

is infected and converted into virus mass according to the mass action law with transmission coefficient $\beta(t)$. Here, the assumption is that all infected host tissue is converted into virus (to the best of our knowledge, it is not known if at the cellular level infected host cells produce 'waste', thus warranting a conversion efficiency parameter). These simplifying assumptions lead to the following model:

$$\frac{\mathrm{d}H}{\mathrm{d}t} = r(t)H - \beta(t)HV \tag{1a}$$

$$\frac{\mathrm{d}V}{\mathrm{d}t} = \beta(t)HV, \tag{1b}$$

where $H(t)$, $V(t) > 0$ for all $t \geq 0$.

During the course of infection, the host becomes increasingly moribund and in the latter stages of infection the host almost completely stops eating and therefore stops growing. This is demonstrated in Section 2.2.2 and supported by additional and closely related findings [24]. Furthermore, we assume that increased viral loads will have greater effect on the host growth rate [24]. We model this by the following integral equation

$$r(t) = r_0 \exp\left(-a \int_0^t V(s)\mathrm{d}s\right) \tag{1c}$$

where r_0 is the maximum host growth rate and a is the host growth reduction rate. Here, the growth rate decreases with the 'experience' of the infection. Note that for mathematical and numerical analyses it is useful to differentiate (1c) with respect to time.

In addition, we assume that as the virus converts an increasing proportion of host mass the infection rate decreases, and tends to zero as the virus proportion approaches a maximal limit, p. We model this by the functional

form

$$\beta(t) = \beta_0 \left(1 - \frac{V(t)}{p(H(t) + V(t))}\right) \tag{1d}$$

where β_0 is the maximum infection rate. This assumption essentially acts to impose a 'carrying capacity' for the pathogen growth within the host since the virus growth is limited by the size of the growing host. Hence, the 'carrying capacity' is not a fixed parameter, but is dynamic with respect to the interactions between the host and the virus. Note that the parameter p acts as an upper limit for the proportion of virus mass within the infected host, as we demonstrated empirically in Section 2.2.2. This is included as not all of the available host mass may be infected (the host head capsule for example), and therefore it is necessary to prescribe this limit via a reduction in the potential carrying capacity. In addition, it should also be noted that since $H(0) >> V(0)$ it follows that $\beta(t) \geq 0$ for all $t \geq 0$.

Linear stability analysis (see Appendix A) of Model (1) reveals that there are an infinite number of locally stable equilibria which lie on the curve

$$\frac{V}{p(H+V)} = 1.$$

Thus, for given growth parameters, r_0, β_0 and a, the equilibria obtained will crucially depend on the mass of the host and the virus dose at the time of infection.

3.2. Parameter Fitting

To fit the within-host infection Model (1) to the within-host virus growth data one must convert the proportion of virus data into virus mass data. To do this we assume that the fraction of sampled DNA that is virus DNA is

equal to the fraction of total host mass that is virus mass. Thus mathematically we have

$$\frac{\text{mass of virus DNA at time } t}{\text{total mass of DNA at time } t} = \frac{\text{mass of virus at time } t}{\text{total mass of infected host at time } t}. \quad (2)$$

Using the host and virus mass data we are able to fit the within-host infection Model (1) to the data and find the associated parameter values (see Appendix B for details). Here, we use some asymptotic properties of the model to find initial estimates of the model parameters and then all parameters are found simultaneously using the initial estimates. Note that we do not prescribe r_0 from the control data, but instead we find it from the simultaneous fitting on the infected data, which therefore takes into account the stochastic differences between treatments. A discussion on prescribing r_0 can be found in the ESM and Table S1. The fitted parameter values are listed in Table 1 and we compare the results of this parameter fitting with the data graphically in Figure 3.

From Figure 3 we see that Model (1) is an excellent fit to both the host and virus data, and we are able to capture all of the growth behaviour. All fits produce the characteristic log-sigmoidal virus growth and the sigmoidal growth of the host. However, due to the exceptionally fast speed of kill of *Se*NPV the deceleration of host growth is almost negligible, which is reflected in the low value of a. In contrast, *Mb*NPV has the largest larvae at the time of death and thus the largest value for a. *Pafl*NPV and *Se*NPV have the largest infection rates, β_0, whilst *Mb*NPV has the smallest infection rate. The extent to which viruses can convert healthy host tissue into virus particles greatly differs between strains, ranging from approximately 2.8% for *Mb*NPV to as much as 22% for *Ac*NPV. The maximum host growth rate, r_0, does not

change considerably between virus treatments. Moreover, the differences we observe in the estimation of the initial masses, H_0 and V_0, are largely due to experimental variation.

3.3. Model Predictions

Using the fitted parameter values we can use Model (1) to predict the effects of varying the initial dose of virus and the size of the host at the time of infection.

In Figure 4 (a) we see that an increase in virus dose leads to a reduction in the yield of virus and host size at the time of host death. At first, this may seem counterintuitive, as one might expect that an increased dose may lead to an increased yield. However, the mechanism behind this phenomenon is a combination of two processes. Firstly, an increased dose has a greater initial negative effect on the host growth rate, resulting in smaller hosts, and therefore the dynamic virus 'carrying capacity' is reduced. Secondly, a greater viral dose increases the initial infection rate and therefore the virus infects a larger proportion of host more quickly, thus causing a decreased yield at death. Furthermore, extensive parameter variation, such as initial host size and host growth rate (not presented here), suggests that this is ubiquitous under our model assumptions.

In Figure 4 (b) we see the effect of varying the size of the host at the time of initial infection. As one might expect, in most cases, as host size increases, the virus yield and the size of host at the time of death both increase. This is because the size increase simply acts as an increased virus carrying capacity and there is a longer period for the virus to replicate before it has a large negative effect on the host growth rate. A similar scenario occurs when the

maximum host growth rate is increased, corresponding to an increase in the host diet or environmental quality (Figure 4 (c)).

The effects of varying virus parameters can be seen in Figure 4 (d)-(f). In Figure 4 (d) we see that, as one might expect, increasing the rate at which the host growth is reduced by the virus infection causes a decrease in host mass which in turn reduces the virus yield. In contrast, one might expect that increasing the infection rate of the virus would increase the virus yield, however, in Figure 4 (e) we see that the opposite is true. This is due to the increase in maximum infection rate (β_0) causing the virus mass to utilise more of the host mass more quickly, resulting in earlier saturation. Therefore, the host is increasingly moribund and suffers from a reduction in growth rate, final host mass and hence a reduction in virus yield. Finally, in Figure 4 (f) we show the effect of varying the zero infection virus proportion, p. Intuitively, we see an increase in proportion of host that the virus can infect causes an increase in viral yield, which in turn reduces the host mass since the host growth rate is reduced by the additional virus mass.

4. Conclusions & Discussion

It is well known that genetically similar virus strains show differences in pathogenicity, speed of kill and yield [19], but here we have shown that they also differ in how they may impact host growth and replicate within it. We have demonstrated empirically that virus infection impedes the growth rate of the host, with some viruses doing so from the early stages of infection, and that this inhibition increases as the infection progresses and has consequences for the outcome of infection. Four genotypically similar strains of

pathogen were found to have differences in traits associated with pathogen fitness (speed of kill, pathogencity), and to impede host growth to differing degrees (parameter a varied by more than an order of magnitude). This led to a lack of correlation between the standard phenotypic traits (speed of kill, pathogenicity) and the efficiency with which the different viruses converted host tissue to virus (for which *Ac*NPV had the highest ratio of virus DNA to host DNA and *Mb*NPV had the lowest).

Using the fitted parameter values from the within-host infection model, we have seen that *Ac*NPV is relatively slow at infecting healthy host tissue. On the other hand, it is clear from the fitted parameter values and the simulations that *Se*NPV is the fastest growing virus, but it does not convert a high ratio of host mass into virus mass. From these parameter-fitting results we can conclude that there is a lack of correlation between initial virus growth rate (β_0) and both the speed of kill and mortality. For example, *Se*NPV does have the highest initial growth rate and it also has the fastest speed of kill and mortality. In contrast, *Pafl*NPV has the slowest speed of kill and lowest mortality, but does not have the lowest initial virus growth rate (this belongs to *Mb*NPV). This would suggest that one cannot predict speed of kill, mortality and virus yield from initial virus growth rate alone and that these pathogen fitness parameters are a result of a number of interacting processes.

Surprisingly, empirical investigation into parasite growth rates has been largely neglected in invertebrate hosts [13]. Our experimental data highlight the initial fast speed at which virus replication occurs. Using an approximation of our mathematical model (B.3), we have shown that the initial virus

growth rate is double exponential ($V(t) \approx e^{e^t}$). This is in stark contrast to previous theory of obligate killing parasites, where more simplistic logistic growth curves have been assumed [15], thus underestimating initial virus growth. Indeed, for the prodigious theory of human diseases the within-host growth of viruses is often shown to be significantly slower ($V(t) \approx e^t$) [25], even before innate or adaptive immune responses slow the within-host spread of disease. This further highlights the differences between the complexity of vertebrate and simplicity of invertebrate hosts and their diseases. The main reason for this difference is the speed at which the host grows. In vertebrate systems host growth is assumed to be constant, since the speed of replication of the pathogen is much faster than the growth rate of the host (Steinmeyer et al. [26] for example).

Interestingly, the fitted statistical model (Figure 2) shows a decline in virus abundance for each of the virus genotypes at approximately 10-20 hours post infection. Why this occurs remains unclear. A possible explanation is a sloughing defence mechanism [27] or simply loss of virus particles on the outer body of the larva from droplet feeding, which illustrates the sensitivity of the molecular method used. It may also be attributed to more complex cellular and humoral mechanisms of immunity and both have been implicated in insect resistance to baculoviruses [28]. In terms of our results, the decline of the virus abundance is likely to have some small effect on the fitted parameter values, in particular underestimating the β_0 values. Further study is clearly required to ascertain the precise cause of the reduction in virus abundance at the early stages of an overt infection and to understand the implications for the host and virus growth dynamics.

From our observations we hypothesise that the speed of kill is strongly dependent on the rate at which the virus grows within the host, how quickly the virus replication rate reaches a plateau (if at all) and how much the virus impedes host growth, but the exact relationship is not immediately obvious. For example, *Pafl*NPV has the slowest speed of kill, whilst in contrast *Mb*NPV has the smallest maximum infection rate, β_0. Therefore, using a simple single parameter to predict the speed of kill is not possible. Furthermore, the biological mechanism behind host death (i.e. timing of host death relative to infection levels) is still relatively undetermined. Previous models have assumed that host death occurs when pathogen fitness is maximised [15]. Ebert and Weisser [15] assumed that the fitness of the obligately killing pathogen, F, is given by

$$F(t_{\text{kill}}) = V(t_{\text{kill}})e^{-mt_{\text{kill}}} \tag{3}$$

where $V(t_{\text{kill}})$ is the number of transmission stages at the time of host death, t_{kill}, and m is the background host mortality. Maximising (3) with respect to the time of host death gives the optimal speed of kill. Ebert and Weisser [15] found that under their model assumptions for the within-host virus growth the optimal killing time approximately corresponded to the period of time during which viral replication rate significantly decreases. However, applying this optimisation to our within-host viral growth model, parameterised for our 4 strains of NPV, results in nonsensical optimal speeds of kill, even for a wide range of background mortalities. This suggests that the speed of kill of baculovirus infections may be more complex than simple pathogen fitness optimisation or that pathogen fitness is not suitably described by (3). Moreover, our empirical data do not support the finding that the killing

time occurs at a point of rapid deceleration in the viral replication rate. In contrast, we find that rapid viral growth, which has been shown in many host-pathogen systems [29], is followed by a prolonged period of deceleration towards a stationary final viral mass (see also Evans et al. [30]). However, this deceleration is less pronounced for some viral strains, in particular *Se*NPV.

To this end, in the ESM we have covaried the speed of kill alongside the other model parameters for two contrasting strains: *Ac*NPV and *Se*NPV, where the former exhibits a strong saturation effect. In each case, a faster speed of kill leads to reduced viral yield and small hosts at the time of death, as one would expect. However, for *Ac*NPV, some parameters are more sensitive to the speed of kill than others - the most sensitive parameters being the initial host mass and viral dose parameters. In contrast, for *Se*NPV, the speed of kill has a large effect on host mass at the time of death and the viral yield for each parameter variation. Therefore, we must conclude that for viruses that exhibit weak saturation, the speed of kill will have a large effect on the viral yield. Moreover, if the speed of kill is greatly altered by either (i) inoculating different insect instars or (ii) changing the viral dose concentration, then viral yield will be greatly affected. Conversely, if the host's environment can affect other model parameters, resulting in different speeds of kill, then there may be no significant change in the viral yield.

Our results show that pathogen infection slows the growth rate of the host, even at the early stages of infection. Surprisingly, there are relatively few studies that empirically demonstrate a reduction in host growth rate (but see Burand and Park [24]), but this is often suggested since parasites cause harm to their hosts as an unavoidable consequence of parasite reproduction.

Our model predicts that a greater virus dose will increase this effect, which agrees with evidence from a similar host-pathogen system [24]. To date, the exact reason behind the reduction of host growth rate is unknown, but a number of possible mechanisms have been put forward. These include host-virus competition for nutrients at the cellular level [24] and the expression of the viral ecdysteroid UDP-glucosyl transferase (EGT) gene which alters host hormones related to host development [31]. Our model does not explicitly state the origins of the growth rate reduction, but we simply incorporate this effect as a composition parameter on the host-virus growth dynamics, which produces a good fit. This enables us to detect differences between virus strains and thus yields, which in terms of transmission in the field is critical, as yield has a direct effect on the abundance of overwintering inoculum.

Our model predicts that larger hosts at the time of infection result in larger viral yields, which supports experimental results of others [30]. Counterintuitively, our model reveals that larger viral doses may decrease viral yield. This result has been discovered experimentally in other closely related systems [30, 32], but this is not always the case [33], perhaps due to the trade-offs between dose, speed of kill and virus yield obscuring this phenomenon. In terms of maximising transmission, the virus will increase its yield with lower doses, but this will trade-off against the probability of infection. Therefore, transmission is likely to be maximised for some intermediate dose. Our result also contrasts with vertebrate within-host theory, where Steinmeyer et al. [26] found that increasing viral dose increased the peak viral load, whilst empirical evidence suggests the contrary, as found in sheep inoculated intranasally with a type O foot-and-mouth disease virus [34]. Here the authors suggested

411 the reason for this is that cell-mediated immune mechanisms responded more
412 quickly to high doses than lower doses, the result being increased inhibition
413 of viral replication.

414 It has been suggested that environmental stress increases host suscep-
415 tibility to infections and reduces host ability to resist parasite growth and
416 reproduction, thus benefiting parasites. This suggestion stems from expected
417 costs of immune defence; hosts in poor condition should have fewer resources
418 to be allocated to immune function. However, the alternative hypothesis
419 for the response to environmental stress is that hosts in poor condition pro-
420 vide fewer resources for parasites and/or suffer higher mortality, leading to
421 reduced parasite growth, reproduction and survival [35]. Under the assump-
422 tion that poorer quality diet results in a lower host growth rate (r_0), our
423 model predicts a reduction in virus yield, and so supports the latter hypoth-
424 esis.

425 Despite the focus of most host-pathogen work concentrating on single in-
426 fections, as we have studied here, molecular techniques have revealed that
427 many infections in insect hosts are caused by several pathogen genotypes
428 which differ phenotypically in their interaction with the host [19]. One ex-
429 ample is the pine beauty moth, *Panolis flammea*, in which a plethora of
430 genetically distinct strains of NPVs have been isolated from a single host.
431 These strains have been found to differ phenotypically in parameters corre-
432 lated with fitness, including the speed with which the pathogen kills the host
433 and the subsequent yields of OBs [19], which may act as non-lethal syner-
434 gists by interacting with secondary virus strains but are not themselves lethal
435 [36]. The simplest assumption would be that competition between genotypes

within a host is a race to gain the greatest share of resources (host tissues) [37], as in the tragedy of the commons [38]. As a consequence, mixed infections may lead to reduced transmission between hosts. Hence, understanding within-host dynamics of multiple infections is essential for understanding the impact of multiple pathogens in the field.

Acknowledgments

This work was supported by an MRC Discipline Hopping Award G0300571 to PKM and RSH. PKM was partially supported by a Royal Society Wolfson Research Merit Award. SMW would like to thank Stephen J. Cornell and Greg Dwyer for some useful discussions, and Tim Carty for providing the insects and diet.

Table

Table 1: Fitted parameter values for the infection model using the method outlined in Section 3.2 for the total host mass and within-host mass growth of *Ac*NPV, *Mb*NPV, *Pafl*NPV and *Se*NPV in third instar larvae of *S. exigua*. The bracketed numbers correspond to the 95% bootstrapped confidence interval for each parameter.

Parameter	*Ac*NPV	*Pafl*NPV	*Mb*NPV	*Se*NPV
Initial Host Mass (g), H_0	5.0642×10^{-3}	5.6441×10^{-3}	5.9695×10^{-3}	4.3949×10^{-3}
	$(4.4941 \times 10^{-3}, 5.6508 \times 10^{-3})$	$(4.0462 \times 10^{-3}, 6.3307 \times 10^{-3})$	$(4.5804 \times 10^{-3}, 7.7104 \times 10^{-3})$	$(3.7634 \times 10^{-3}, 4.5878 \times 10^{-3})$
Virus Dose (g), V_0	1.3089×10^{-9}	3.5492×10^{-9}	9.1399×10^{-9}	2.4957×10^{-10}
	$(7.2990 \times 10^{-10}, 3.3345 \times 10^{-9})$	$(1.9431 \times 10^{-9}, 6.9817 \times 10^{-8})$	$(5.6659 \times 10^{-9}, 2.1487 \times 10^{-8})$	$(1.7004 \times 10^{-10}, 5.1954 \times 10^{-10})$
Max. Host Growth Rate (h^{-1}), r_0	3.7446×10^{-2}	2.3584×10^{-2}	3.4451×10^{-2}	3.6758×10^{-2}
	$(3.4601 \times 10^{-2}, 4.2140 \times 10^{-2})$	$(2.0334 \times 10^{-2}, 3.2734 \times 10^{-2})$	$(2.8663 \times 10^{-2}, 4.1988 \times 10^{-2})$	$(3.4622 \times 10^{-2}, 3.7876 \times 10^{-2})$
Zero Infection Virus Proportion, p	2.1588×10^{-1}	4.9161×10^{-2}	2.8096×10^{-2}	4.6904×10^{-2}
	$(1.3742 \times 10^{-1}, 3.5856 \times 10^{-1})$	$(3.8357 \times 10^{-2}, 6.5778 \times 10^{-2})$	$(1.6406 \times 10^{-2}, 4.3981 \times 10^{-2})$	$(4.5363 \times 10^{-2}, 1.7088 \times 10^{-1})$
Max. Infection Rate ($g^{-1}h^{-1}$), β_0	16.750	16.530	6.9231	20.151
	(13.760,17.022)	(14.142,21.722)	(5.4750,7.7177)	(16.354,21.331)
Host Growth Reduction Rate (h^{-1}), a	1.9390	7.9301	31.813	5.0346
	(0.9933,4.5449)	(2.3150,22.454)	(20.025,128.84)	(1.2807,5.5024)

Appendix A. Model Analysis

Since $r(t) \to 0$ as $t \to \infty$ the nullclines are given by $\beta(t) = 0$ for both $H' = V' = 0$, and thus are given by

$$\frac{V}{p(H+V)} = 1.$$

Hence, the nullclines for both of the coupled differential equations completely overlap and therefore the equilibria, which are given by the intersection of the nullclines, are defined by a curve.

Proof of our claims on stability will be reported elsewhere; here we simply sketch the details. Straightforward linear stability analysis reveals the existence of a centre manifold. The long-term behaviour critically depends on the initial conditions. The system will blow up if the initial dose is sufficiently large relative to the initial host size, that is, if $\beta(0) < 0$. However, given that the virus dose is small compared to the initial host size it is biologically reasonable to assume that $\beta(0) > 0$. Then, since the equilibrium is given by $\beta(t) = 0$ it can be shown that the system tends to the equilibrium. Moreover, the fast and slow dynamics are calculable for the manifold.

Appendix B. Parameter Fitting

Here we outline the method used for the parameter fitting of the mathematical model (1). The results of these methods are listed in Table 1 and shown graphically in Figure 3. For this we use a two-stage process:

1. Since we have assumed that in the absence of virus the host initially grows exponentially, we fit the curve

$$H(t) = H(0)e^{r_0 t} \tag{B.1}$$

where $H(0) = H_{0_{\text{cont}}}$, to the initial growth phase of the control data, thus giving the initial estimate of the maximum growth rate r_0 and the initial host mass $H_{0_{\text{cont}}}$ for the control data. We then use r_0 and the total mass of the infected hosts data to find the initial size of the host, H_0.

To find the initial estimates of the maximum infection rate, β_0, and the initial dose, V_0, we use the fact that initially the amount of virus within the host is small. Hence we may approximate model (1) by

$$\frac{\mathrm{d}H}{\mathrm{d}t} = r_0 H \tag{B.2a}$$

$$\frac{\mathrm{d}V}{\mathrm{d}t} = \beta_0 HV. \tag{B.2b}$$

Solving (B.2) we obtain

$$V(t) = V_0 \exp\left\{\frac{\beta_0 H_0}{r_0}\left(e^{r_0 t} - 1\right)\right\} \tag{B.3}$$

where $V(0) = V_0$, for the initial growth of the virus. Hence one can use (B.3) to fit to the initial part of the virus data to find the initial parameter estimates for β_0 and V_0.

It is not possible to find initial estimates for the host growth reduction rate, a, and the zero infection virus proportion, p, using techniques similar to those above. Therefore, we fit the model to both the total host mass and virus mass data simultaneously by making use of the previously found initial parameter estimates.

2. The set of six initial parameter estimates are then fitted to the data simultaneously where the previously found parameter estimates are used as 'good' initial guesses. Since the data exhibit growing variance over

the course of the infection, we perform a log-transformation to account for this [39].

All fitting is achieved by the method of least squares using a modified Levenberg-Marquardt algorithm [40] and implemented in MATLAB®, using a Runge-Kutta method for solving the differential equations numerically. This fitting method, often referred to as "trajectory matching" [41] or "model calibration" [42], has been successful in fitting in other biological datasets (see Harrison [43] for example). Our method works well here since the time-series has little process noise and we assume that all the error is from observation, but for noisy data more complex methods can be used, such as a gradient matching method [44].

The bootstrapped confidence intervals are calculated from 10000 bootstrapped data sets (with replacements), to which the model is fitted using the parameter estimates as initial guesses.

References

[1] P. J. Hudson, A. P. Dobson, D. Newborn, Prevention of population cycles by parasite removal, Science 208 (1998) 2256–2258.

[2] E. T. Borer, P. R. Hosseini, E. W. Seabloom, A. P. Dobson, Pathogen-induced reversal of native dominance in a grassland community, P. Natl. Acad. Sci. USA 104 (2007) 5473–5478.

[3] S. Blanford, B. H. K. Chan, N. Jenkins, D. Sim, R. J. Turner, A. F. Read, M. B. Thomas, Fungal pathogen reduces potential for malaria transmission, Science 308 (2005) 1638–1641.

[4] C. E. Mitchell, A. G. Power, Release of invasive plants from fungal and viral pathogens, Nature 421 (2003) 625–627.

[5] P. Daszak, A. A. Cunningham, A. D. Hyatt, Emerging infectious diseases of wildlife - threats to biodiversity and human health, Science 287 (2000) 443–449.

[6] G. Dwyer, J. Dushoff, J. S. Elkinton, S. A. Levin, Pathogen-driven outbreaks in forest defoliators revisited: Building models from experimental data, Am. Nat. 156 (2000) 105–120.

[7] J. C. de Roode, A. B. Pedersen, M. D. Hunter, S. Altizer, Host plant species affects virulence in monarch butterfly parasites, J. Anim. Ecol. 77 (2008) 120–126.

[8] R. Antia, M. Lipsitch, Mathematical models of parasite responses to host immune defences, Parasitology 115 (1997) S155–S167.

[9] S. P. Ellner, L. E.Jones, L. D. Mydlarz, C. D. Harvell, Within-host disease ecology in the sea fan *Gorgonia ventalina*: Modeling the spatial immunodynamics of a coral-pathogen interaction, Am. Nat. 170 (2007) E143–E161.

[10] R. Antia, B. R. Levin, R. M. May, Within-host population dynamics and the evolution and maintenance of microparasite virulence, Am. Nat. 144 (1994) 457–472.

[11] S. Alizon, M. van Baalen, Multiple infections, immune dynamics, and the evolution of virulence, Am. Nat. 172 (2008) E150–E168.

[12] A. S. Perelson, Modelling viral and immune system dynamics, Nat. Rev. Immunol. 2 (2002) 28–36.

[13] R. Hamilton, M. Siva-Jothy, M. Boots, Two arms are better than one: parasite variation leads to combined inducible and constitutive innate immune responses, Proc. R. Soc. B 275 (2008) 937–945.

[14] M. T. Siva-Jothy, Y. Moret, J. Rolff, Insect immunity: An evolutionary ecology perspective, Adv. Insect Physiol. 32 (2005) 1–48.

[15] D. Ebert, W. W. Weisser, Optimal killing for obligate killers: The evolution of life histories and virulence of semelparous parasites, Proc. R. Soc. B 264 (1997) 985–991.

[16] L. A. Lacey, H. K. Kaya (Eds.), Field Manual of Techniques in Invertebrate Pathology: Application and Evaluation of Pathogens for Control of Insects and other Invertebrate Pests, Springer, Netherlands, second edition, 2007.

[17] F. R. Hunter-Fujita, P. F. Entwistle, H. F. Evans, N. E. Crook, Insect viruses and pest management, John Wiley & Sons, 1998.

[18] J. P. Burden, R. D. Possee, S. M. Sait, L. A. King, R. S. Hails, Phenotypic and genotypic characterisation of persistent baculovirus infections in populations of the cabbage moth (*Mamestra brassicae*) within the british isles, Arch. Virol. 151 (2006) 635–649.

[19] D. J. Hodgson, A. J. Vanbergen, A. D. Watt, R. S. Hails, J. S. Cory, Phenotypic variation between naturally co-existing genotypes of a lepidopteran baculovirus, Evol. Ecol. Res. 3 (2001) 687–701.

[20] M. D. Ayres, S. C. Howard, J. Kuzio, M. Lopez-Ferber, R. D. Possee, The complete DNA sequence of *Autographa californica* nuclear polyhedrosis virus, Virology 202 (1994) 586–605.

[21] W. F. J. Ijkel, E. A. van Strien, J. G. M. Heldens, R. Broer, D. Zuidema, R. W. Goldbach, J. M. Vlak, Sequence and organisation of the *Spodoptera exigua* multicapsid nucleoployhedrovirus genome, J. Gen. Virol. 80 (1999) 3289–3304.

[22] P. R. Hughes, N. A. M. V. Beek, H. A. Wood, A modified droplet feeding method for rapid assay of *Bacillus thuringiensis* and baculoviruses in noctuid larvae, J. Invertebr. Pathol. 48 (1986) 187–192.

[23] P. Schmid-Hempel, Evolutionary ecology of insect immune defenses, Annu. Rev. Entomol. 50 (2005) 529–551.

[24] J. P. Burand, E. J. Park, Effect of nuclear polyhedrosis virus infection on the development and pupation of gypsy moth larvae, J. Invertebr. Pathol. 60 (1992) 171–175.

[25] R. M. Ribeiro, L. Qin, L. L. Chavez, D. Li, S. G. Self, A. S. Perelson, Estimation of the initial viral growth rate and basic reproductive number during acute HIV-1 infection, J. Virol. 84 (2010) 6096–6102.

[26] S. H. Steinmeyer, C. O. Wilke, K. M. Pepin, Methods of modelling viral disease dynamics across the within- and between-host scales: the impact of virus dose on host population immunity, Proc. R. Soc. B 365 (2010) 1931–1941.

[27] B. A. Keddie, G. W. Aponte, L. E. Volkman, The pathway of infection of *Autographa californica* nuclear polyhedrosis virus in an insect host, Science 243 (1989) 1728–1730.

[28] J. O. Washburn, B. A. Kirkpatrick, L. E. Volkman, Insect protection against viruses, Nature 383 (1996) 767–767.

[29] M. C. Otterstatter, J. D. Thomson, Within-host dynamics of an intestinal pathogen of bumble bees, Parasitology 133 (2006) 749–761.

[30] H. F. Evans, C. J. Lomer, D. C. Kelly, Growth of nuclear polyhedrosis virus in larvae of the cabbage moth, *Mamestra brassicae L.*, Arch. Virol. 70 (1981) 207–214.

[31] K. R. Wilson, D. R. O'Reilly, R. S. Hails, J. S. Cory, Age-related effects of the autographa californica multiple nucleopolyhedrovirus *egt* gene in the cabbage looper (*Trichoplusia ni*), Biol. Control 19 (2000) 57–63.

[32] D. J. Hodgson, A. J. Vanbergen, S. E. Hartley, R. S. Hails, J. S. Cory, Differential selection of baculovirus genotypes mediated by different species of host food plant, Ecol. Lett. 5 (2002) 512–518.

[33] J. S. Cory, B. M. Green, R. K. Paul, F. R. Hunter-Fujita, Genotypic and phenotypic diversity of a baculovirus population within an individual insect host, J. Invertebr. Pathol. 89 (2005) 101–111.

[34] G. J. Hughes, R. P. Kitching, M. E. J. Woolhouse, Dose-dependent responses of sheep inoculated intranasally with a type o foot-and-mouth disease virus, J. Comp. Path. 127 (2002) 22–29.

[35] O. Seppälä, K. Liljeroos, A. Karvonen, J. Jokela, Host condition as a constraint for parasite reproduction, Oikos 117 (2008) 749–753.

[36] B. M. Bonsall, The impact of non-lethal synergists on the population and evolutionary dynamics of host-pathogen interactions, J. Theor. Biol. 262 (2010) 567–575.

[37] R. M. May, M. A. Nowak, Coinfection and the evolution of parasite virulence, Proc. R. Soc. B 261 (1995) 209–215.

[38] G. Hardin, The tragedy of the commons, Science 162 (1968) 1243–1248.

[39] A. Grafen, R. Hails, Modern Statistics for the Life Sciences, Oxford University Press, 2002.

[40] R. Fletcher, A Modified Marquardt Subroutine for Non-Linear Least Squares, Technical Report AERE-R–6799, Atomic Energy Research Establishment, Harwell (England), 1971.

[41] B. M. Bolker, Ecological Models and Data in R, Princeton University Press, 2008.

[42] B. E. Kendall, C. J. Briggs, W. W. Murdoch, P. Turchin, S. P. Ellner, E. McCauley, R. M. Nisbet, S. N. Wood, Why do populations cycle? A synthesis of statistical and mechanistic modeling approaches, Ecology 80 (1999) 1789–1805.

[43] G. W. Harrison, Comparing predator-prey models to luckinbill's experiment with didinium and paramecium, Ecology 76 (1995) 357–374.

[44] S. P. Ellner, Y. Seifu, R. H. Smith, Fitting population dynamic models to time-series data by gradient matching, Ecology 83 (2002) 2256–2270.

Figure 1

Mean weight of third instar larvae infected with *Ac*NPV, *Mb*NPV, *Pafl*NPV, *Se*NPV and uninfected control. The lines show the fitted values for (a) *Ac*NPV ($\log \text{weight} = -2.2827 + 0.0104 \times \text{time} + 1.4605 \times 10^{-4} \times \text{time}^2 - 1.3546 \times 10^{-6} \times \text{time}^3$), (b) *Mb*NPV ($\log \text{weight} = -2.3446 + 0.0180 \times \text{time} - 4.9347 \times 10^{-6} \times \text{time}^2 - 4.0265 \times 10^{-7} \times \text{time}^3$), (c) *Pafl*NPV ($\log \text{weight} = -2.3832 + 0.0183 \times \text{time} - 9.0041 \times 10^{-5} \times \text{time}^2 + 1.1677 \times 10^{-7} \times \text{time}^3$), (d) *Se*NPV ($\log \text{weight} = -2.2662 + 0.0146 \times \text{time} - 4.7435 \times 10^{-5} \times \text{time}^2 + 1.8663 \times 10^{-7} \times \text{time}^3$) and (e) uninfected controls ($\log \text{weight} = -2.2718 + 0.0119 \times \text{time} + 1.3297 \times 10^{-4} \times \text{time}^2 - 9.8279 \times 10^{-7} \times \text{time}^3$). In (f) the mean weights are plotted for the various treatments, along with fitted lines for uninfected controls ($\log \text{weight} = -2.2829 + 0.01644 \times \text{time}$), *Ac*NPV ($\log \text{weight} = -2.2973 + 0.01444 \times \text{time}$), *Mb*NPV ($\log \text{weight} = -2.2963 + 0.01527 \times \text{time}$), *Pafl*NPV ($\log \text{weight} = -2.2947 + 0.01131 \times \text{time}$) and *Se*NPV ($\log \text{weight} = -2.2392 + 0.01219 \times \text{time}$).

Figure 2

The within-host growth of (a) *Ac*NPV, (b) *Mb*NPV, (c) *Pafl*NPV and (d) *Se*NPV in third instar larvae of *S. exigua* as measured by the proportion of total DNA represented by viral DNA. The lines show the fitted values for *Ac*NPV ($\log \text{proportion} = -4.6000 - 0.3706 \times \text{time} + 0.0181 \times \text{time}^2 - 2.7824 \times 10^{-4} \times \text{time}^3 + 1.8302 \times 10^{-6} \times \text{time}^4 - 4.4369 \times 10^{-9} \times \text{time}^5$), *Mb*NPV ($\log \text{proportion} = -5.4454 - 0.0473 \times \text{time} + 0.0010 \times \text{time}^2 + 2.0390 \times 10^{-5} \times \text{time}^3 - 3.3223 \times 10^{-7} \times \text{time}^4 + 1.1557 \times 10^{-9} \times \text{time}^5$), *Pafl*NPV ($\log \text{proportion} = -5.6825 - 0.1018 \times \text{time} + 0.0062 \times \text{time}^2 - 8.3174 \times$

643 $10^{-5} \times \text{time}^3 + 4.3875 \times 10^{-7} \times \text{time}^4 - 8.0036 \times 10^{-10} \times \text{time}^5$) and *Se*NPV
644 (log proportion $= -6.2862 - 0.2996 \times \text{time} + 0.0172 \times \text{time}^2 - 2.8257 \times 10^{-4} \times$
645 $\text{time}^3 + 1.9346 \times 10^{-6} \times \text{time}^4 - 4.8002 \times 10^{-9} \times \text{time}^5$).

646 **Figure 3**

647 The total host mass and within-host mass growth of (a) *Ac*NPV, (b)
648 *Mb*NPV, (c) *Pafl*NPV and (d) *Se*NPV in third instar larvae of *S. exigua*.
649 The asterisks denote total host mass, plus signs denote virus mass from the
650 experimental data and the solid and dashed lines show the results of the
651 fitted Model (1) for the parameter values in Table 1. Note that the virus
652 axes are in a $\log_{10}$ scale.

653 **Figure 4**

654 The effects of the virus parameters in infections. Here we run simulations
655 of Model (1) using the parameters in Table 1 for *Ac*NPV. In each graph the
656 total host mass (solid line) and the virus yield (dashed line) at the time of
657 host death is plotted against (a) virus dose, V_0, (b) initial host mass, H_0,
658 (c) maximum host growth rate, r_0, (d) host growth reduction rate, a, (e)
659 maximum infection rate, β_0, and (f) zero infection virus proportion, p. The
660 time to death is 160 hours. Note that qualitatively similar results hold for
661 *Mb*NPV, *Se*NPV and *Pafl*NPV.

Figure 1

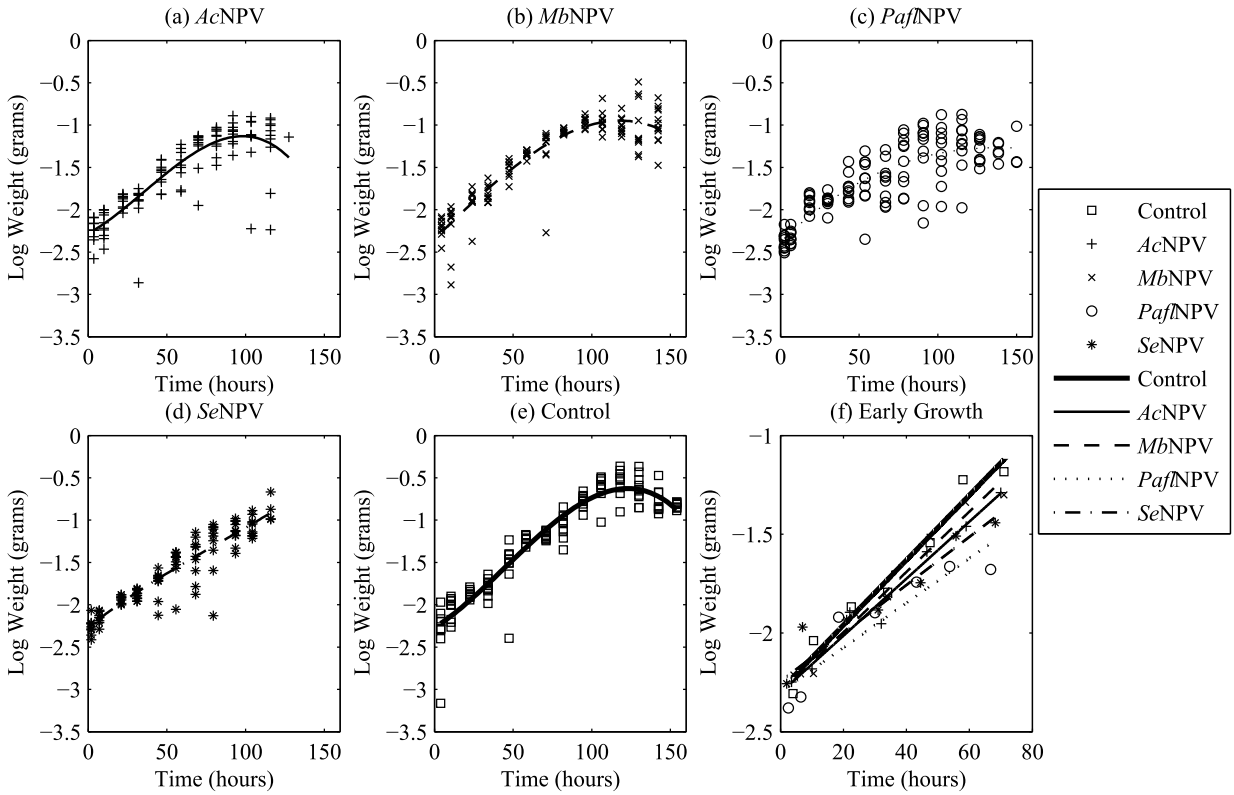
(a) AcNPV
(b) MbNPV
(c) PaflNPV
(d) SeNPV
(e) Control
(f) Early Growth
Log Weight (grams)
Time (hours)
Control
AcNPV
MbNPV
PaflNPV
SeNPV

Figure 2

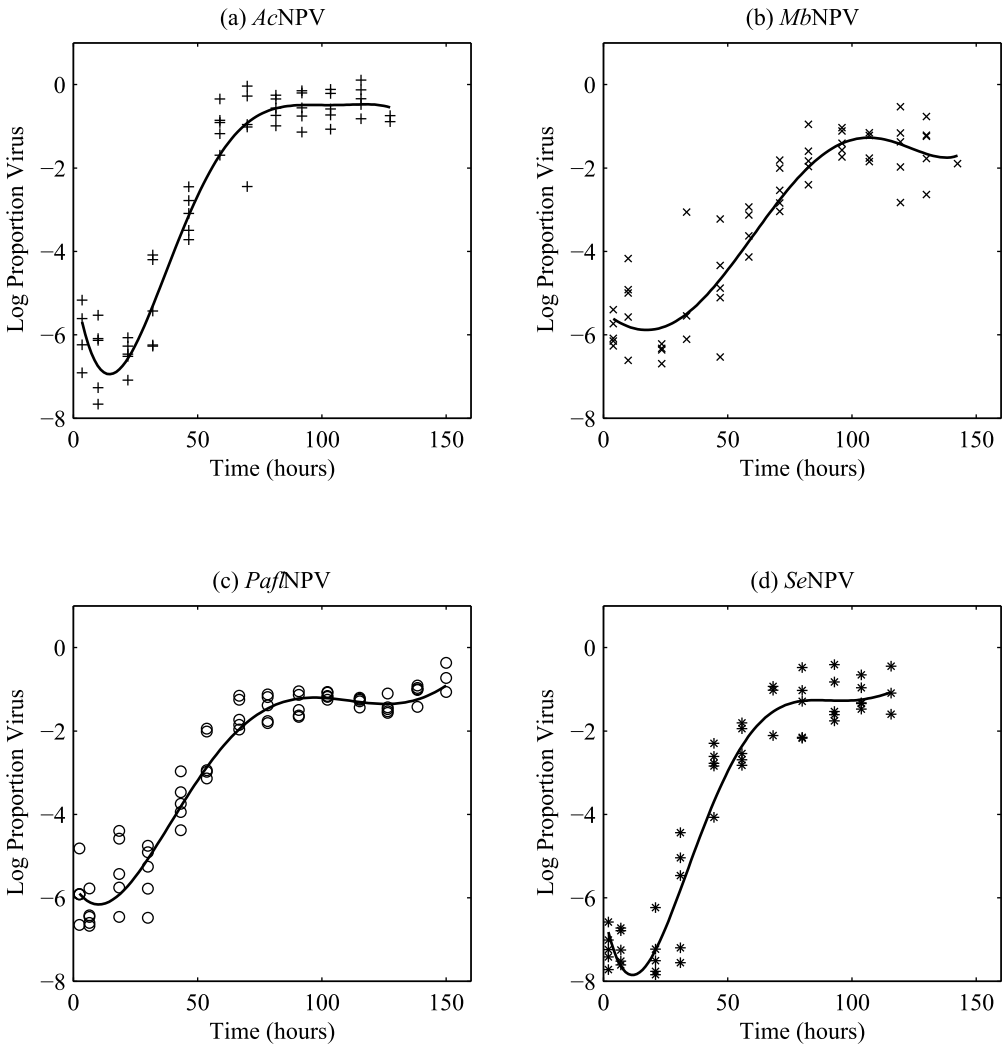
(a) AcNPV
(b) MbNPV
(c) PaflNPV
(d) SeNPV
Log Proportion Virus
Time (hours)
0
−2
−4
−6
−8
0
50
100
150

Figure 3

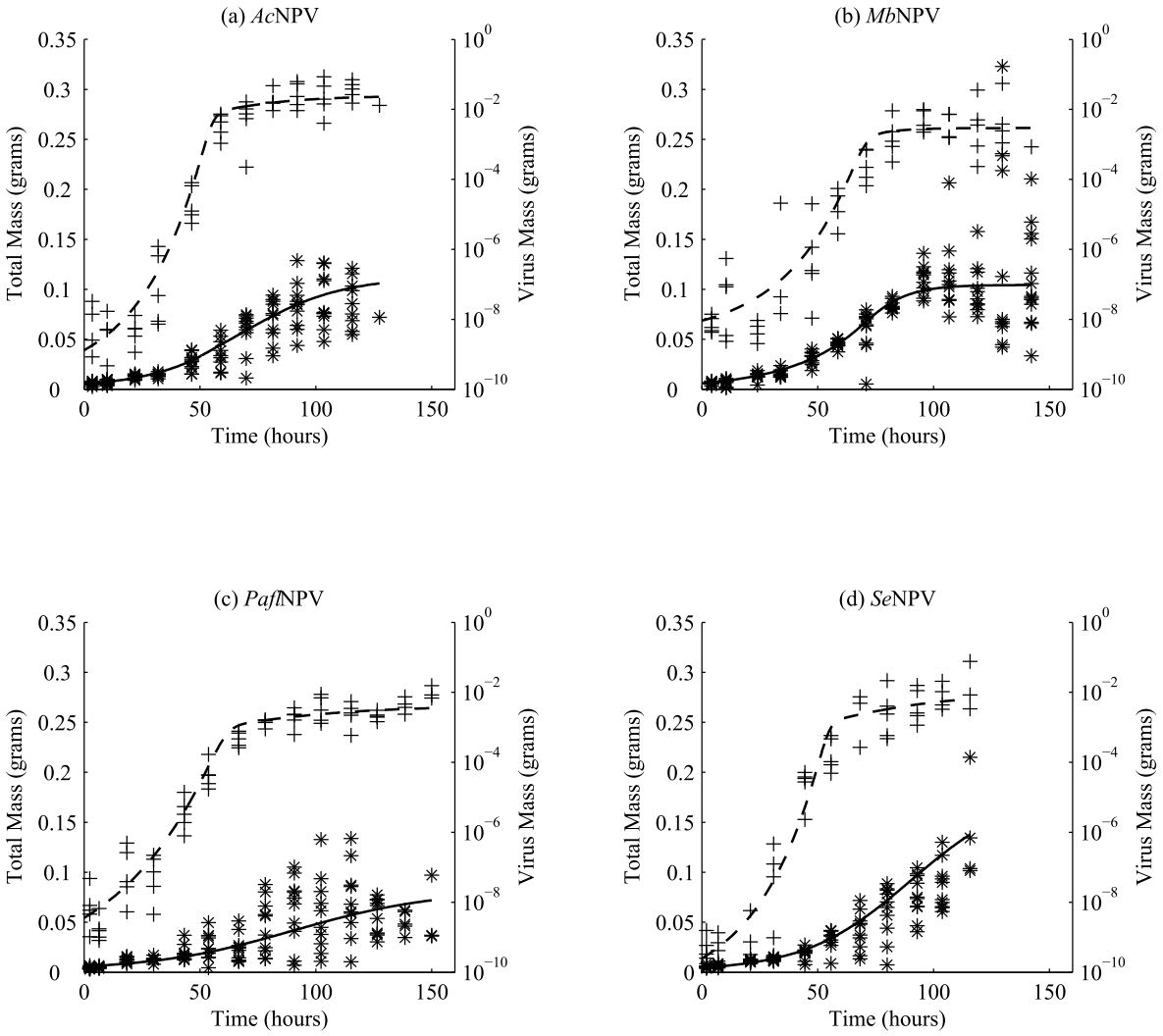
(a) AcNPV
(b) MbNPV
(c) PaflNPV
(d) SeNPV
Total Mass (grams)
Virus Mass (grams)
Time (hours)
0.35
0.3
0.25
0.2
0.15
0.1
0.05
0
10^{0}
10^{-2}
10^{-4}
10^{-6}
10^{-8}
10^{-10}
0
50
100
150

Figure 4

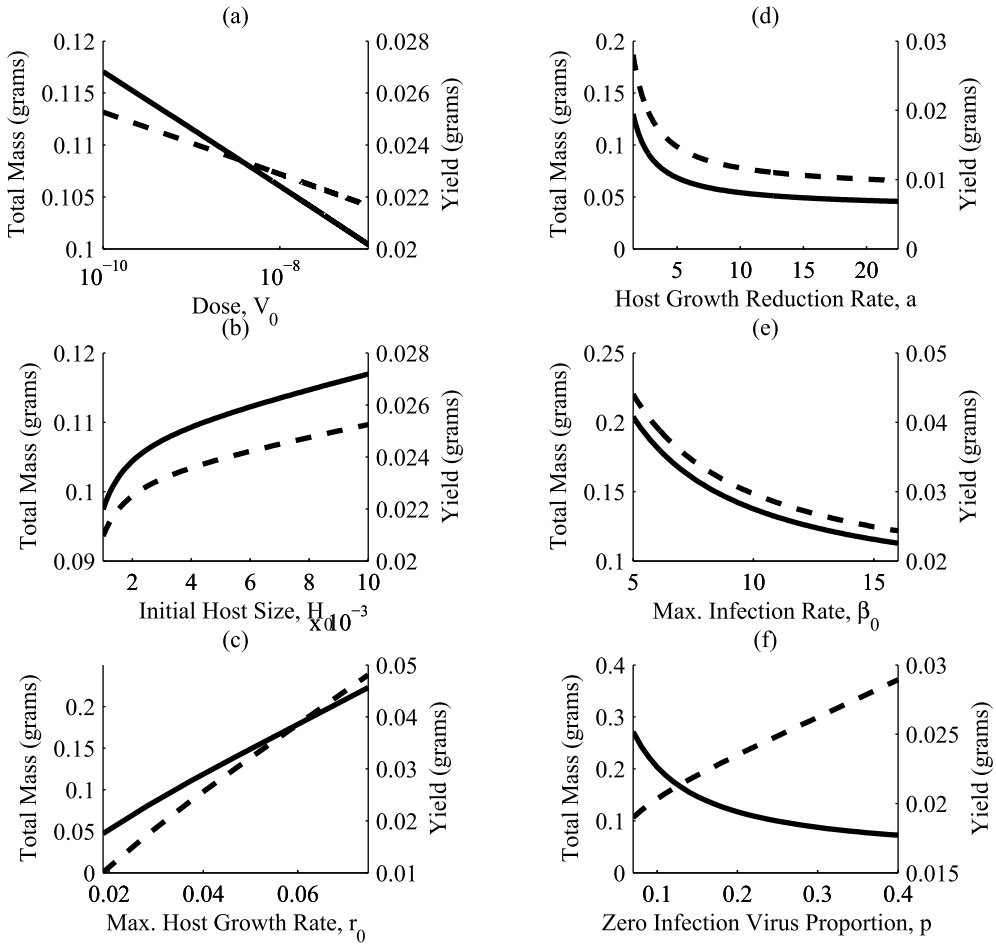
(a)
Total Mass (grams)
Yield (grams)
Dose, V_0
(b)
Initial Host Size, H_0
x 10^-3
(c)
Max. Host Growth Rate, r_0
(d)
Host Growth Reduction Rate, a
(e)
Max. Infection Rate, β_0
(f)
Zero Infection Virus Proportion, p

Modelling the within-host growth of viral infections in insects: Electronic supplementary material

Steven M. White[1,2]*, John P. Burden[1], Philip K. Maini[2,3] and Rosemary S. Hails[1]

May 15, 2012

[1] Centre for Ecology & Hydrology, Maclean Building, Benson Lane, Crowmarsh Gifford, Wallingford, Oxfordshire, OX10 8BB, United Kingdom.

[2] Centre for Mathematical Biology, Mathematical Institute, University of Oxford, 24-29 St Giles', Oxford, Oxfordshire, OX1 3LB, United Kingdom.

[3] Oxford Centre for Integrative Systems Biology, Department of Biochemistry, South Parks Road, Oxford, OX1 3QU, United Kingdom.

*Email: smwhit@ceh.ac.uk

1 Insect and virus stocks

Spodoptera exigua larvae were obtained from Syngenta (Jeallotts Hill, UK) in 2003 and reared in continuous culture on artificial diet [1]. This population was shown to be free from persistent baculovirus infections by PCR and RT-PCR for the viral polyhedrin gene using total insect DNA as a template.

Four different baculoviruses were used in this study; the Oxford strain of *Mamestra brassicae* nucleopolyhedrovirus (*Mb*NPV) [2], *Panolis flammea* nucleopolyhedrovirus (*Pafl*NPV) variant 4 [3], *Autographa californica* nucleopolyhedrovirus (*Ac*NPV) strain C6 [4] and *Spodoptera exigua* nucleopolyhedrovirus (*Se*NPV) [5]. Stocks of each virus were made by dosing third instar *S. exigua* larvae with 10^8 occlusion bodies (OBs) by diet plug feeding [6], and purifying the virus by density gradient centrifugation [1]. The titre of the purified virus stock was estimated using an Improved Neubauer haemocytometer (B.S. 748, Weber, UK) and the virus stored at -20°C. Virus stocks were re-counted before each use.

2 Statistical Methods

The data were analysed using generalised linear modelling techniques (GLIM version 3.77, Royal Statistical Society, 1985). For the analysis of mortality all explanatory variables (virus concentration, virus, block) and their interactions were fitted to the mortality data. A binomial error structure was assumed, which was substantiated by subsequent inspection of the scale parameter [7]. The contribution of each term was tested for significance and non-significant terms removed to leave the minimal adequate model. Box-Cox transformations indicated an inverse transformation was required for data on time to larval death.

3 DNA Extraction & Quantification

DNA (insect and viral) was extracted from the frozen larvae by first thawing them and then disrupting them using a manual tissue grinder. Total DNA was then extracted from this material using a DNEasy mini kit (Qiagen). The DNA was eluted from the column into

200μl of elution buffer and quantified by spectrophotometry at 260nm and 280nm. Extracted DNA was stored at -20°C. DNA was extracted from 5 of the larvae harvested at each time point.

Viral DNA was quantified by real-time PCR using a Rotor Gene RG-3000 (Corbett Research) and a CAS-1200 liquid handling system (Corbett Research). Primer pairs were designed, specific to the sequence of each virus, to amplify a region of approximately 200 base pairs (bp) from the viral ie1 gene (*Ac*IE1-1 AAGGTGTGGTGGGCCAGTTT, *Ac*IE1-2 TGGTCGGAGAACCTGTTGGA, *Mb*IE1-1 TTGCTTCCGAAGGACCACAA, *Mb*IE1-2 ATCCCGTGTCGAGCAAATGA, *Pf*IE1-1 CGTCAACGGCATCAACAACA, *Pf*IE1-2 TGGCAGCTCCTTTTCCAACA, *Se*IE1-1 TCGACAACAGCGGCATCTTT, *Se*IE1-2 CGGTAGCGTTCGATGGTGAC).

Each real-time PCR reaction mixture consisted of Platinum SYBR Green qPCR SuperMix-UDG (Invitrogen) (10μl), sterile distilled water (6.2μl), BSA (1μl), and the appropriate primers (10pmol/μl, 0.4μl of each primer) to which was added 2μl of the extracted total DNA. The reaction profile was a single cycle of 50°C for 2 minutes, followed by 40 cycles of 95°C for 15 seconds, 57°C for 15 seconds and 72°C for 15 seconds. This was followed by a stage in which the temperature was raised from 57°C to 99°C in 1°C intervals to allow for subsequent melt curve analysis.

For each sample duplicate real-time PCR reactions were run and each PCR run included duplicate negative controls in which the template DNA was replaced by 2μl of sterile distilled water. For the quantification of the samples, genomic DNA from the appropriate virus was used to generate a standard curve. Viral genomic DNA was purified by caesium chloride gradient purification of DNA released from virus particles [6]. For each set of quantification reactions a series of five decimal dilutions of the viral genomic DNA was set up using the CAS-1200 system. This dilution series was made from an initial sample of the virus DNA which had been quantified by spectrophotometry at 260nm and 280nm. Standard samples were also run in duplicates. A standard curve was generated based on this dilution series using the software associated with the RG-3000, which also quantified the samples based on

this curve. Standard curves with an R2 value of less than 0.99 were rejected. Samples were only regarded as giving a positive real-time PCR result if the take-off point of the reaction was before that seen with any primer dimers produced in the negative control reactions and a product with the appropriate denaturation temperature was seen on the melt-curve analysis.

An average of two duplicates was taken to be the quantification for a given sample. As the total amount of DNA in the PCR reaction was known (2μl of known concentration in each reaction) the proportion of this which was viral could therefore be calculated.

4 Consequences of Censoring Technique

One drawback of our sampling method is that data points towards the end of the time series are censored. Some insects died before the final time point, so those censored at the final time point are selected from those that survived. There are likely to be yield differences depending upon time of death, and therefore the final sub-sample will be biased. It is unclear how this affects our results, but it is most likely to affect host-pathogen systems where one compares a virus with a high degree of variance in the speed of kill to a virus with a low degree of variance (which does not apply here) as this will influence the degree of bias. To combat this, the only solution would be to monitor the growth of virus in individual larvae by subsampling from the same insect throughout the course of infection. However, there are a number of technical issues with sampling tissue and accurately estimating total virus abundance within the host without killing the insect.

5 Virus Growth Rate

By equation (B.3), the model predicts that the initial growth rate is double exponential. This is faster than the single exponential growth rate that is common in many other infection models. Indeed, using an approximation to equation (B.3) such that

$$V(t) \approx V_0 \exp\{\beta_0 H_0 t\} \tag{1}$$

equation (1) underpredicts the growth of virus (see Figure S2).

6 Prescribing r_0

In the main text we show the results of the model fitting whereby all model parameters are fitted to the data from infected individuals simultaneously. This is done so that we account for stochastic differences between treatments and to allow the value to be and emergent property of the simultaneous fitting. However, r_0, the maximum host growth, is the innate parameter of host growth and should be independent of the infection. Hence, an alternative fitting strategy could be to fit r_0 from the initial control data (i.e. before any pupation effects occur), fix this parameter and fit the remaining parameters as described by the previous method. In this section, we carry out this fitting and discuss the implications.

The results of prescribing r_0 are shown in Table S1. Comparing this result to our previous result (Table 1 in the main text), we see that the biggest effect is on the host growth reduction rate, a. Here we see a large increase in this parameter value compared to the previous fitting. This difference would suggest that, by not fitting fixing the maximum host growth rate to the control data, the fitting method underestimates the host growth slow-down caused by the virus.

7 Dependence on the Speed of Kill

In Figures S3 and S4 we have further explored the impacts of the speed of kill on the host mass (left hand column) and yield (right hand column) for all 6 parameters (rows) in the model for two contrasting virus strains: *Ac*NPV and *Se*NPV. The results are discussed in the main text Discussion.

References

[1] F. R. Hunter-Fujita, P. F. Entwistle, H. F. Evans, N. E. Crook, Insect viruses and pest management, John Wiley & Sons, 1998.

[2] J. P. Burden, R. D. Possee, S. M. Sait, L. A. King, R. S. Hails, Phenotypic and genotypic characterisation of persistent baculovirus infections in populations of the cabbage moth (*Mamestra brassicae*) within the british isles, Arch. Virol. 151 (2006) 635–649.

[3] D. J. Hodgson, A. J. Vanbergen, A. D. Watt, R. S. Hails, J. S. Cory, Phenotypic variation between naturally co-existing genotypes of a lepidopteran baculovirus, Evol. Ecol. Res. 3 (2001) 687–701.

[4] M. D. Ayres, S. C. Howard, J. Kuzio, M. Lopez-Ferber, R. D. Possee, The complete DNA sequence of *Autographa californica* nuclear polyhedrosis virus, Virology 202 (1994) 586–605.

[5] W. F. J. Ijkel, E. A. van Strien, J. G. M. Heldens, R. Broer, D. Zuidema, R. W. Goldbach, J. M. Vlak, Sequence and organisation of the *Spodoptera exigua* multicapsid nucleoployhedrovirus genome, J. Gen. Virol. 80 (1999) 3289–3304.

[6] L. A. King, R. D. Possee, The Baculovirus Expression System; A Laboratory Guide, Chapman & Hall, 1992.

[7] M. Aitken, D. Anderson, B. Francis, J. Hinde, Statistical Modelling in GLIM, Oxford Statistical Science Series 4, Oxford University Press, Oxford, 1989.

Table S1: Fitted parameter values for the infection model using the method outlined in Section 3.2 with the r_0 prescribed by fitting it to the first 7 census points of the control data. See Table 1 in the main manuscript for a comparison.

Parameter	*Ac*NPV	*Paft*NPV	*Mb*NPV	*Se*NPV
Initial Host Mass (g), H_0	4.437×10^{-3}	3.512×10^{-3}	5.5512×10^{-3}	3.763×10^{-3}
Virus Dose (g), V_0	1.25×10^{-9}	4.56×10^{-9}	9.72×10^{-9}	5.19×10^{-10}
Max. Host Growth Rate (h^{-1}), r_0	3.642×10^{-2}	3.642×10^{-2}	3.642×10^{-2}	3.642×10^{-2}
Zero Infection Virus Proportion, p	2.439×10^{-1}	4.058×10^{-2}	2.726×10^{-2}	1.709×10^{-1}
Max. Infection Rate ($g^{-1}h^{-1}$), β_0	19.859	18.130	6.881	16.354
Host Growth Reduction Rate (h^{-1}), a	1.116	26.775	37.104	1.281

(a) (b)

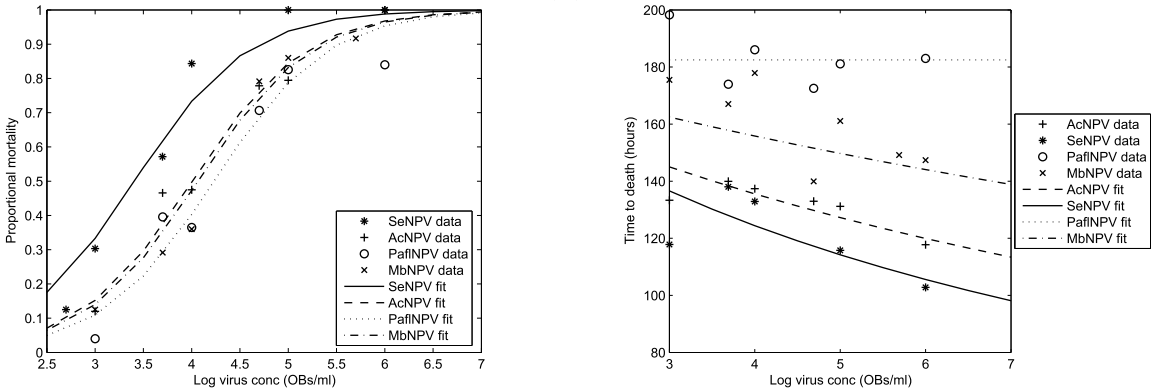

Figure S1: In (a) dose-mortality curves for *Ac*NPV, *Mb*NPV, *Pafl*NPV and *Se*NPV. The lines show the fitted values for *Ac*NPV and *Mb*NPV (logit $= -6.948 + 1.725 \times$ log(virus conc)), *Pafl*NPV (logit $= -7.2812 + 1.725 \times \log$(virus conc)) and *Se*NPV (logit $= -5.802 + 1.725 \times \log$(virus conc)) and proportional mortality is given by $p = 1/(1+(1/e^{\text{logit}}))$. In (b) mean time to death vs dose curves for *Ac*NPV, *Mb*NPV, *Pafl*NPV and *Se*NPV. The lines show the fitted values for *Ac*NPV (time to death $= 1/(0.005454 + 0.0004807 \times \log$ dose)), *Mb*NPV (time to death $= 1/(0.00537152 + 0.0002615 \times \log$ dose)), *Pafl*NPV (time to death $=$ 182.48) and *Se*NPV (time to death $= 1/(0.0051692 + 0.0007172 \times \log$ dose)). The analysis carried-out was inverse transformed with normal errors.

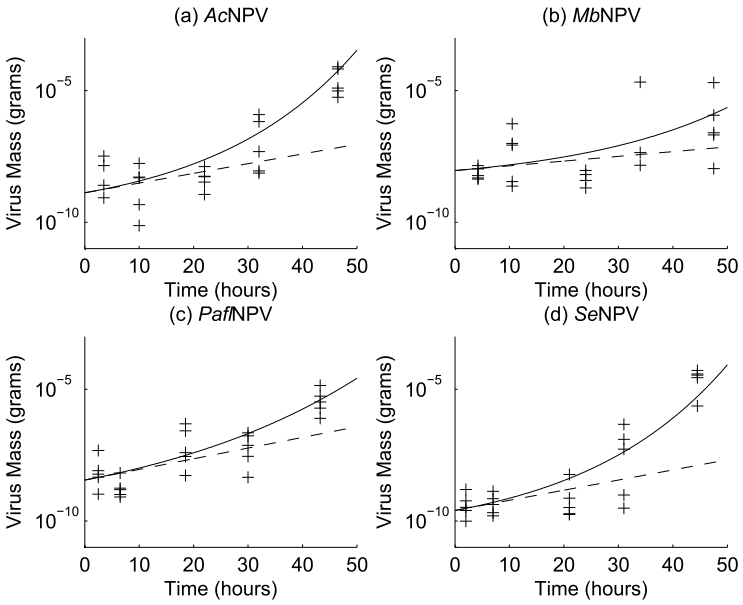

Figure S2: Comparisons of the two approximations for the initial growth of virus. Solid lines denote the double exponential approximation function (B.3); dashed lines denote the exponential approximation function (1). All parameters used are taken from the full ODE model for each virus strain.

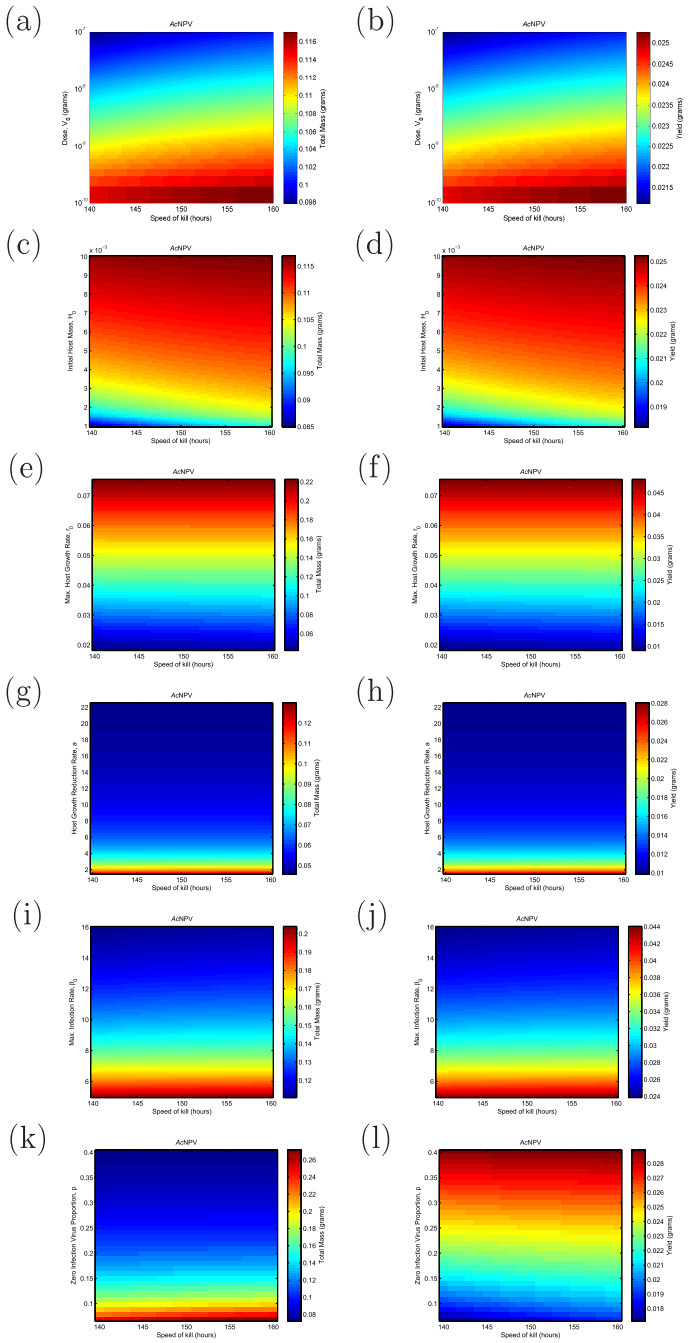

Figure S3: Quantifying the effects of the speed of kill on host mass and yield of virus for *Ac*NPV. Here we run simulations of Model (1) using the parameters in Table 1 for *Ac*NPV. We have plotted the total host mass (left hand column) and viral yield (right hand column) for all 6 parameters (rows). The colours indicate the masses for each parameter and speed of kill combination.

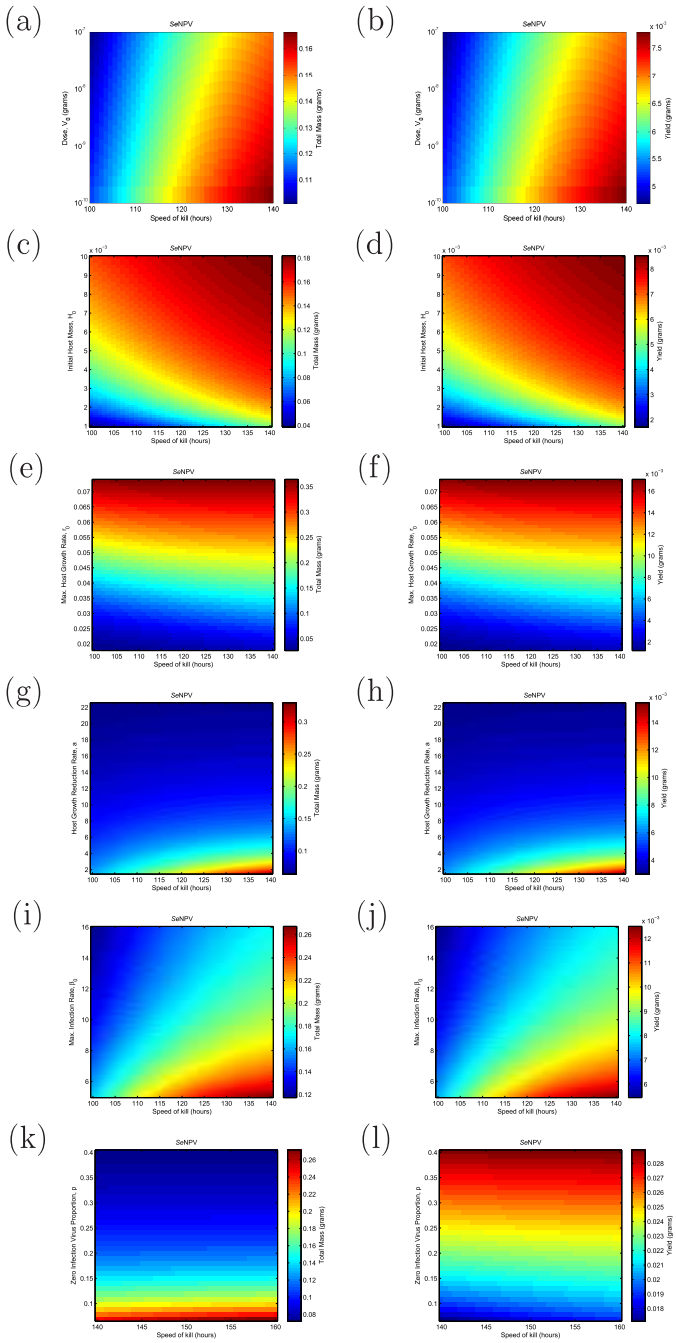

Figure S4: Quantifying the effects of the speed of kill on host mass and yield of virus for *Se*NPV. Here we run simulations of Model (1) using the parameters in Table 1 for *Se*NPV. We have plotted the total host mass (left hand column) and viral yield (right hand column) for all 6 parameters (rows). The colours indicate the masses for each parameter and speed of kill combination.